Assessing PET Parameters in Oncologic ^{18}F-FDG Studies

Ismet Sarikaya[1] and Ali Sarikaya[2]

[1]Department of Nuclear Medicine, Kuwait University Faculty of Medicine, Kuwait City, Kuwait; and [2]Department of Nuclear Medicine, Trakya University Faculty of Medicine, Edirne, Turkey

PET imaging, particularly oncologic applications of ^{18}F-FDG, has become a routine diagnostic study. To better describe malignancies, various PET parameters are used. In ^{18}F-FDG PET studies, SUV_{max} is the most commonly used parameter to measure the metabolic activity of the tumor. In obese patients, SUV corrected by lean body mass (SUL), and in pediatric patients, SUV corrected by body surface area, are recommended. Metabolic tumor volume is an important parameter to determine the local and total tumor burden. Total lesion glycolysis (SUV_{mean} × metabolic tumor volume) provides information about averages. Some treatment response assessment protocols recommend using the SUV_{peak} or SUL_{peak} of the tumor. Tumor-to-liver ratio and tumor–to–blood-pool ratio are helpful when comparing studies for treatment response assessment. Dual–time-point PET imaging with retention index can help differentiate malignant from benign lesions and may help detect small lesions. Dynamic ^{18}F-FDG PET imaging and quantitative analysis can measure the metabolic, phosphorylation, and dephosphorylation rates of lesions but are mainly used for research purposes. In this article, we will review the currently available PET parameters in ^{18}F-FDG studies with their importance, uses, limitations, and reasons for erroneous results.

Key Words: PET; parameter; ^{18}F-FDG; oncology; SUV

J Nucl Med Technol 2020; 48:278–282
DOI: 10.2967/jnmt.119.236109

PET imaging is based on detecting 2 simultaneously released 511-keV photons after a positron (emitted from the injected radiotracer in the body) moves in the tissue for a distance (positron range) until it reaches rest mass and then collides with a tissue electron, causing an annihilation reaction. PET imaging is a high-technology product but still has certain limitations related to various factors such as the noncollinearity of 511-keV photons, positron range, and parallax error, which affect its sensitivity and spatial resolution in detecting small lesions (*1–3*). Noncollinearity causes less of a problem in small-animal PET scanners, and therefore, small-animal PET scanners have a higher spatial resolution than standard human PET scanners (~1 vs. 4–6 mm) (*4*).

PET imaging, particularly with ^{18}F-FDG, has been used commonly since the introduction of PET/CT fusion cameras in the early 2000s. PET images are visually assessed and also supported by quantitative parameters. Currently, the most commonly used PET parameter is SUV in oncologic ^{18}F-FDG studies. The other parameters include SUV normalized by lean body mass (SUL), metabolic tumor volume (MTV), total lesion glycolysis (TLG), tumor-to-liver and tumor–to–blood-pool ratios, retention index in dual–time-point PET studies, and dynamic PET imaging parameters. Various other parameters are available with various radiotracers in oncologic, neurologic, and cardiac PET studies, which will not be discussed in this review article. However, most of the PET parameters described in this article can also be used in other oncologic PET studies, with different SUVs in normal tissues and thresholds in differentiating malignant from benign lesions.

SUV

SUV is a commonly used PET parameter to measure the uptake of various radiopharmaceuticals, mainly ^{18}F-FDG, in normal tissues and lesions (*5–7*). SUV is simply the ratio of the activity concentration in the target tissue or lesion to the activity concentration in the whole body:

$$\text{SUV} = \text{kBq/cm}^3\,(\text{lesion or target tissue})/(\text{decay} - \text{corrected injected activity}\,(\text{MBq})/\text{patient weight}\,(\text{kg}))$$

This equation assumes that the injected activity is uniformly distributed in the whole body and that 1 cm^3 of tissue weighs 1 g (*8*). Activity in the lesion or target tissue is decay-corrected.

Because of metabolic heterogeneity or irregular tumor borders, SUV_{max} is used instead SUV_{mean}. SUV_{max} is the maximum voxel value of SUV in the tumor. SUV_{max} does not represent the whole tumor metabolic burden and is sensitive to image noise (*9*).

SUV generally accurately estimates the degree of uptake of radiopharmaceuticals in lesions and normal tissues but is affected by various patient, biologic, and technical factors that can cause over- or underestimation of the activity in lesions and tissues. Examples include suboptimal patient preparation; high blood glucose and insulin levels; diabetic status; body mass index; age; sex; significant extravasation of activity;

Received Sep. 4, 2019; revision accepted Oct. 30, 2019.
For correspondence or reprints contact: Ismet Sarikaya, Department of Nuclear Medicine, Faculty of Medicine, Kuwait University, P.O. Box 24923, Safat, Kuwait 13110.
E-mail: isarikaya99@yahoo.com
Published online Dec. 6, 2019.

image acquisition and reconstruction parameters; conditions during the postinjection uptake period; inaccurate entry of weight, height, and injected activity; clock synchronization errors; inaccurate entry of injection time and imaging start time; effect of CT contrast material on attenuation-corrected PET images; patient and organ motion; and other diseases and medications affecting ^{18}F-FDG uptake (Figs. 1–3) (*8,10–15*).

In the normalization of SUV, usually the patient's total weight is used. However, in obese people, SUV is overestimated in lesions and normal tissues (Fig. 1) (*16,17*) because ^{18}F-FDG is distributed mainly in nonfat tissues and the percentage of adipose tissue is high in obese people, with minimal ^{18}F-FDG accumulation in the fat. Use of SUL, instead of normalization by total weight, is recommended in obese patients (*16,17*). SUL also allows for a better comparison of the PET images of a patient whose weight has changed significantly between PET studies. Weight changes, particularly loss, are common in oncologic patients because of treatments or disease progression. SUV will be overestimated when the patient is overweight or obese and underestimated when the patient is underweight or has cachexia. There are various ways of measuring lean body mass. It can be calculated through predictive equations using height and body weight (*18*). However, semidirect measurements of lean body mass such as bioelectrical impedance analysis, dual-energy x-ray absorptiometry, CT, and MRI can provide more accurate results (*19*). Using a more accurate method to measure lean body mass will provide a more accurate SUL. However, all these methods have certain limitations, advantages, and disadvantages. CT and MRI are the most precise and accurate methods but are costly and complex to operate (*19*). Bioelectrical impedance analysis and dual-energy x-ray absorptiometry are more accessible, easier to use, and less costly (*19*). CT is not recommended in pregnant women and in children because of radiation exposure. MRI is not suitable for patients with metallic parts. A standard method for calculating lean body mass will allow more accurate comparison of PET studies obtained at different institutes. SUL can be measured either directly by simply entering the patient's lean body mass instead of total weight or indirectly by calculating it from SUV with the following formula:

$$\text{SUL} = (\text{SUV} \times \text{lean body mass})/\text{total weight}.$$

In heavy patients, the SUVs of blood, liver, and spleen were up to twice those of lighter patients (*16*). In our recent study, the SUVs of the liver and blood pool were significantly higher in obese patients than in patients with a normal body mass index, and SUL_{mean} was approximately 75% of SUV_{mean} in patients with a normal body mass index and 55% of SUV_{mean} in obese patients (*20*). For comparison, the percentage of fat is 20%–25% of total body weight in young women with a normal body mass index and 38%–40% in young obese women (*21*). If SUL is going to be used routinely, standard values (thresholds for differentiating benign from malignant lesions, and normal liver and blood-pool values) should be determined. In our recent study, SUL_{mean} in the liver and blood pool were 2.2 and 1.8, respectively, in patients with a normal body mass index and were similar in obese patients (*20*). SUL is not affected by body weight or lean body mass (*20*).

Studies assessing SUV in children found that SUVs in the liver and tumor are lower than those in adults (*22,23*). SULs in children are also lower than normal adult values (*23*). These studies recommended using a body-surface-area–based SUV in children (*22,23*). The lower SUV and SUL in children than in adults could be due to the higher amount of brown fat in children, which could competitively reduce the uptake of activity in other normal tissues and lesions.

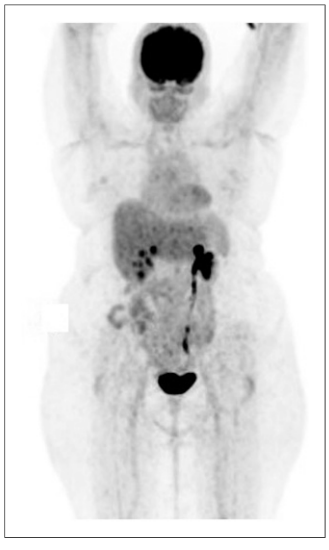

FIGURE 1. Effect of body weight on SUV. Image shows whole-body ^{18}F-FDG PET maximum-intensity projection of obese !patient (59-y-old woman; weight, 114 kg; height,165 cm; lean body mass, 59.4 kg). SUV_{mean} in liver and blood pool are 5 and 4.1, respectively, which are above normal values and higher than visually seen activity in liver and blood pool. SUL is 2.6 in liver and 2.1 in blood pool. Overweight and obesity can also cause overestimation of SUV in lesions.

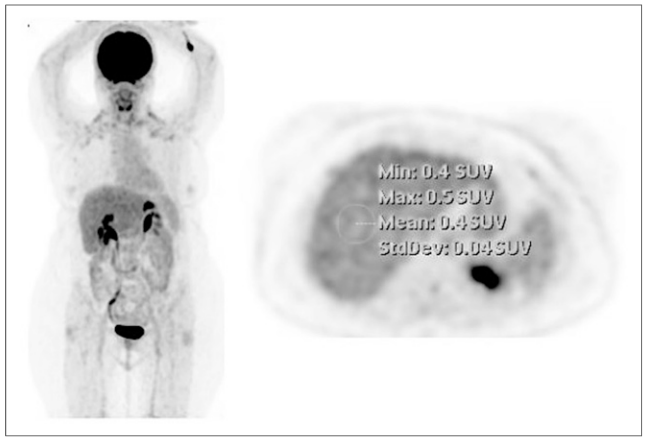

FIGURE 2. ^{18}F-FDG PET whole-body maximum-intensity projection and transaxial selected PET slice from liver in adult patient with erroneously low SUV (liver SUV_{mean}, 0.4). Inaccurate entering of injected ^{18}F-FDG activity in PET computer (3,000 MBq instead of 300 MBq) caused significantly low SUV in liver and other tissues in this patient. When measured SUV does not match visual findings, it is important to check patient data in PET computer (weight, height, and injected dose). In addition, as activity is decay-corrected for SUV, accuracy of injection and imaging start times should also be checked. Clocks used in department should be synchronized.

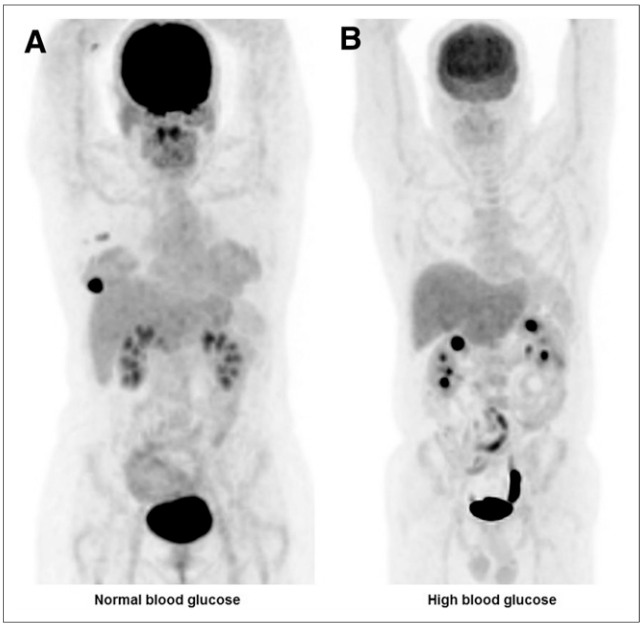

FIGURE 3. Effect of high blood glucose on brain ^{18}F-FDG uptake in ^{18}F-FDG PET whole-body maximum-intensity projection images. (A) A 48-y-old woman with recently diagnosed breast cancer (fasting blood glucose, 97.2 mg/dL; SUV_{max} in right frontal cortex, 19.6; SUV_{mean} in liver, 3.6; SUV_{mean} in blood pool, 3.2). (B) A 52-y-old man with pancreatic lesion (fasting blood glucose, 216 mg/dL; SUV_{max} in right frontal cortex, 5; SUV_{mean} in liver, 2.7; SUV_{mean} in blood pool, 1.5). Visually, there is diffusely decreased uptake in brain. Patient does not have cranial symptoms. Compare brain activity with liver uptake and bladder activity in both cases.

There is minimal ^{18}F-FDG uptake in white fat, but brown fat shows moderate to high ^{18}F-FDG uptake (*24,25*). Brown fat is a tissue that produces heat to regulate body temperature. Severe brown fat uptake of significant extent may cause a competitive reduction in ^{18}F-FDG uptake in the tumor, resulting in visually low uptake and a quantitatively low SUV. Brown fat is usually seen in greater amounts in children, and some adults also show brown fat activity, particularly underweight people in a cold environment. Rarely is brown fat seen in overweight and obese patients, and in such cases, SUL may not be accurate if there is a significant distribution of activity in brown fat.

Hyperglycemia is well known to reduce ^{18}F-FDG uptake in the tumor and brain (Fig. 3). Brain ^{18}F-FDG uptake and SUV gradually decrease with an increasing blood glucose level and are approximately 20% less than normal in low hyperglycemia (111–120 mg/dL) and 65% less than normal in significant hyperglycemia (>200 mg/dL) (*12*). Brain and tumors both show a high expression of glucose transporters 1 and 3. Hyperglycemia reduces ^{18}F-FDG SUV in the tumor to an extent that may be similar to the above reductions in the brain. Measured tumor SUV_{max} can be multiplied by reduction factors of 1.25, 1.5, 2, 2.5, and 2.8 for the blood glucose ranges of 111–120, 121–140, 141–160, 161–200, and at least 201 mg/dL, respectively, to correct SUV in hyperglycemic adults (*12*). Including the brain in whole-body images can provide a better idea of the effect of hyperglycemia with ^{18}F-FDG uptake and SUV (Fig. 3) (*12*).

MTV AND TLG

MTV is an important parameter that measures the metabolically active tumor volume (local and total tumor burden). Tumor tissue may contain necrotic or dead tissues or atelectasis, and the volume of the tumor may therefore look larger on CT than on PET. PET shows uptake in the metabolically active parts of the tumor and in inflammation and lack of uptake in dead tissues, necrosis, and atelectasis. There are various methods (threshold-based and algorithm-based) to measure MTV via computer programs (*9,26*). Fixed-absolute-threshold methods may be more suitable to assess the prognostic value of MTV, and algorithm-based methods seem to be better than fixed-threshold methods to predict tumor response or accurately delineate the tumor for radiotherapy applications (*9*). If a computer program is not available to measure MTV, gross manual measurement in each slice can be performed, which is time-consuming. TLG is obtained by multiplying SUV_{mean} by MTV (*27*). SUV_{mean} is obtained by placing a region of interest around the hottest part of the tumor.

MTV and TLG have prognostic value in a variety of malignancies, and high MTV and TLG predict a worsening prognosis (*28–30*). MTV and TLG are reported to correlate better with histopathologic response than does SUV_{max} (*31*). SUV_{max} is a single value reflecting only the highest pixel activity; however, TLG reflects 2 parameters: average whole-tumor metabolic activity and volume of the tumor. MTV and TLG are also important when adjusting the dose of treatments. If there is metabolic heterogeneity in the tumor, TLG may be overestimated because SUV_{mean} is obtained by placing a region of interest over the hottest part of the tumor. Moreover, TLG can be calculated accurately by measuring total lesion activity and multiplying it by MTV. MTV and TLG appear to be useful parameters but have not been commonly used in routine clinical practice.

UPTAKE RATIO

Tumor–to–reference-region activity ratio is another PET parameter. The most commonly used reference regions are liver and blood pool (*32–35*). Tumor SUV_{max}–to–liver SUV_{mean} ratio and tumor SUV_{max}–to–blood-pool SUV_{mean} ratio are generally used. In liver and blood pool, SUV_{mean} provides more accurate results than SUV_{max}. The SUV_{peak} of the tumor can also be used (*36*). SUV_{peak} is the average value within a small, fixed-size region of interest in the hottest part of the tumor. PERCIST, a grading system for PET lesions in oncology, recommends using SUL_{peak} from the tumor when comparing 2 studies (*37,38*). Tumor-to-liver and tumor–to–blood-pool ratios are usually used to compare 2 PET studies for treatment response assessment (*35,37–39*). In treatment response assessment of lymphomas, the Deauville 5-point scale is recommended (1, no uptake in the tumor;

2, tumor uptake equal to or less than mediastinum; 3, tumor uptake greater than mediastinum but equal to or less than liver; 4, tumor uptake moderately greater than liver; and 5, tumor uptake markedly greater than liver) (*35,39*).

Uptake ratios may provide a better understanding of the metabolic activity of the tumor than can a numeric value (SUV). For example, describing the metabolic activity of the tumor as 3 times the metabolic activity of the normal liver may give a better idea than providing a numeric value (tumor SUV, 9). These parameters are also not affected by patient weight or injected activity. Tumor–to–blood-pool ratio may be preferred over tumor-to-liver ratio because treatments and diseases may affect the metabolic activity of the liver. On the other hand, reduced renal function can cause increased blood-pool activity, which may reduce the accuracy of tumor–to–blood-pool ratio.

High blood glucose generally reduces tumor ^{18}F-FDG uptake, but there are various reports on its effect on liver and blood-pool activity. Per our recent assessment, hyperglycemia does not affect liver and blood-pool activity (*12,40,41*). However, various other studies and a recent meta-analysis study reported that hyperglycemia increases liver and blood-pool activity (*42–46*). Thus, in hyperglycemic patients, tumor-to-liver or tumor–to–blood-pool activity ratio should be used carefully.

DUAL–TIME-POINT PET IMAGING AND RETENTION INDEX

Dual–time-point PET imaging (obtaining both early standard and delayed PET images) has been used extensively in various cancers to differentiate benign from malignant lesions. In addition to visual assessment, retention index (percentage difference in SUV between early and delayed images) is calculated in these studies as follows:

$$\text{Retention index}\,(\%) = 100\times[(\text{SUV}_{\max}\text{delayed} - \text{SUV}_{\max}\text{early})/\text{SUV}_{\max}\text{early}].$$

Dual–time-point PET imaging improved the diagnostic accuracy for malignant lung nodules (*47*). However, in lung lesions whose size and $\text{SUV}_{\max}$ are greater than 10 mm and 2.5, respectively, authors did not recommended dual–time-point ^{18}F-FDG PET imaging to differentiate between malignant and benign lesions (*48*). Tian et al. found a significant differences in retention index between malignant and benign bone lesions: approximately 18 versus 7, respectively (*49*). In the breast, dual–time-point imaging improved PET/CT accuracy in patients with a suspected breast malignancy over single–time-point imaging, demonstrating increasing ^{18}F-FDG uptake over time in breast tumors and decreasing uptake in benign lesions (*50*). In grading brain tumors, $\text{SUV}_{\max}$ and SUV_{peak} from delayed images were more efficient than those from early images (*51*). Delayed imaging may also allow better detection of small lesions due to improved contrast between the lesion and the background (*52*).

DYNAMIC PET IMAGING

Dynamic PET imaging with ^{18}F-FDG and quantification approaches helps to estimate the rates of glucose transport, phosphorylation, and dephosphorylation in the tumor (*53,54*). Compartment modeling is used to analyze the dynamic imaging data. A 2-tissue-compartment model was first described by Sokoloff et al. (*55*). Tracer flows between the blood compartment and tissue compartments. Four transport rates (k_1, k_2, k_3, and k_4) describe the exchange of the tracer between blood and tissue compartments (*54*). In ^{18}F-FDG studies, k_1 reflects the influx, k_2 the efflux, k_3 the phosphorylation rate, and k_4 the dephosphorylation rate of the glucose analog (*54*). Patlak graphical analysis is an approach for calculation of the metabolic rate of glucose (*56*). The metabolic rate of ^{18}F-FDG can then be calculated as influx rate (K_i) × [plasma glucose/lumped constant] (*54*). The lumped constant is the ratio of ^{18}F-FDG uptake to glucose uptake and is not exactly known for tumors (*54*). K_i can be calculated using the rate constants of the 2-tissue-compartment model and the formula $[k_1 \times k_3/k_2 + k_3]$ (*54*). Dynamic PET with quantification is time-consuming and requires dedicated evaluation software and expertise and is usually applied in research. When software is not available to measure dynamic PET parameters, ^{18}F-FDG uptake rate can be grossly assessed by obtaining dynamic images over the tumor (e.g., 1 min, 60 frames) after the injection of ^{18}F-FDG and generating a time–activity curve by placing a same-sized region of interest in the same slice of the tumor in all frames and applying decay correction.

^{18}F-FDG dynamic PET imaging has been studied in various malignancies for differentiating malignant from benign lesions and grading malignant tumors (*57–59*). In a study of soft-tissue sarcomas, SUV, k_1, K_i, and fractal dimension were higher in sarcomas than in benign tumors, and SUV, vascular fraction, k_3, K_i, and fractal dimension were higher in recurrent lesions than in scar tissues (*59*). In another study, k_3, K_i, and metabolic rate of ^{18}F-FDG were significantly higher in higher-grade tumors, progesterone-receptor negative tumors, and highly proliferating tumors, as well as in triple-negative and hormone-receptor negative/HER2-positive subtypes (*53*). It also appears that K_i was significantly higher in node-positive than in node-negative disease (*53*).

CONCLUSION

Various PET parameters are available for ^{18}F-FDG studies. We have summarized them in this article, with their importance, uses, limitations, and reasons for erroneous results.

DISCLOSURE

No potential conflict of interest relevant to this article was reported.

REFERENCES

1. Levin CS, Hoffman EJ. Calculation of positron range and its effect on the fundamental limit of positron emission tomography system spatial resolution. *Phys Med Biol.* 1999;44:781–799.
2. Muehllehner G, Karp JS. Positron emission tomography imaging: technical considerations. *Semin Nucl Med.* 1986;16:35–50.

3. Jones T, Townsend D. History and future technical innovation in positron emission tomography. *J Med Imaging (Bellingham).* 2017;4:011013.
4. Yao R, Lecomte R, Crawford ES. Small-animal PET: what is it, and why do we need it? *J Nucl Med Technol.* 2012;40:157–165.
5. Leskinen-Kallio S, Någren K, Lehikoinen P, et al. Uptake of ^{11}C-methionine in breast cancer studied by PET: an association with the size of S-phase fraction. *Br J Cancer.* 1991;64:1121–1124.
6. Adler LP, Blair HF, Williams RP, et al. Grading liposarcomas with PET using [^{18}F]FDG. *J Comput Assist Tomogr.* 1990;14:960–962.
7. Lucignani G, Paganelli G, Bombardieri E. The use of standardized uptake values for assessing FDG uptake with PET in oncology: a clinical perspective. *Nucl Med Commun.* 2004;25:651–656.
8. Kinahan PE, Fletcher JW. Positron emission tomography-computed tomography standardized uptake values in clinical practice and assessing response to therapy. *Semin Ultrasound CT MR.* 2010;31:496–505.
9. Im HJ, Bradshaw T, Solaiyappan M, et al. Current methods to define metabolic tumor volume in positron emission tomography: which one is better? *Nucl Med Mol Imaging.* 2018;52:5–15.
10. Boellaard R. Standards for PET image acquisition and quantitative data analysis. *J Nucl Med.* 2009;50(suppl 1):11S–20S.
11. Lindholm P, Minn H, Leskinen-Kallio S, et al. Influence of the blood glucose concentration on FDG uptake in cancer: a PET study. *J Nucl Med.* 1993;34:1–6.
12. Sarikaya I, Sarikaya A, Sharma P. Assessing the effect of various blood glucose levels on ^{18}F-FDG activity in the brain, liver, and blood pool. *J Nucl Med Technol.* 2019;47:313–318.
13. Boellaard R, Krak NC, Hoekstra OS, et al. Effects of noise, image resolution, and ROI definition on the accuracy of standard uptake values: a simulation study. *J Nucl Med.* 2004;45:1519–1527.
14. Jaskowiak CJ, Bianco JA, Perlman SB, et al. Influence of reconstruction iterations on ^{18}F-FDG PET/CT standardized uptake values. *J Nucl Med.* 2005;46:424–428.
15. Soret M, Bacharach SL, Buvat I. Partial-volume effect in PET tumor imaging. *J Nucl Med.* 2007;48:932–945.
16. Zasadny KR, Wahl RL. Standardized uptake values of normal tissues at PET with 2-[fluorine 18]fluoro-2-deoxy-D-glucose: variations with body weight and a method for correction. *Radiology.* 1993;189:847–850.
17. Sugawara Y, Zasadny KR, Neuhoff AW, et al. Reevaluation of the standardized uptake value for FDG: variations with body weight and methods for correction. *Radiology.* 1999;213:521–525.
18. Hume R. Prediction of lean body mass from height and weight. *J Clin Pathol.* 1966;19:389–391.
19. Devriese J, Beels L, Maes A, et al. Review of clinically accessible methods to determine lean body mass for normalization of standardized uptake values. *Q J Nucl Med Mol Imaging.* 2016;60:1–11.
20. Sarikaya I, Albatineh A, Sarikaya A. Re-visiting SUV-weight and SUV-lean body mass in FDG PET studies. *J Nucl Med Technol.* October 11, 2019 [Epub ahead of print].
21. Gallagher D, Heymsfield SB, Heo M, et al. Healthy percentage body fat ranges: an approach for developing guidelines based on body mass index. *Am J Clin Nutr.* 2000;72:694–701.
22. Sugawara Y, Shulkin BL, Zasadny KR, et al. Standardized uptake values in pediatric patients: variations with patient characteristics and methods for correction [abstract]. *J Nucl Med.* 2000;41(suppl):196P.
23. Yeung HW, Sanches A, Squire OD, et al. Standardized uptake value in pediatric patients: an investigation to determine the optimum measurement parameter. *Eur J Nucl Med Mol Imaging.* 2002;29:61–66.
24. Hany TF, Gharehpapagh E, Kamel EM, et al. Brown adipose tissue: a factor to consider in symmetrical tracer uptake in the neck and upper chest region. *Eur J Nucl Med Mol Imaging.* 2002;29:1393–1398.
25. Cohade C, Osman M, Pannu HK, et al. Uptake in supraclavicular area fat ("USA-Fat"): description on ^{18}F-FDG PET/CT. *J Nucl Med.* 2003;44:170–176.
26. Paulino AC, Johnstone PA. FDG-PET in radiotherapy treatment planning: Pandora's box? *Int J Radiat Oncol Biol Phys.* 2004;59:4–5.
27. Larson SM, Erdi Y, Akhurst T, et al. Tumor treatment response based on visual and quantitative changes in global tumor glycolysis using PET-FDG imaging: the visual response score and the change in total lesion glycolysis. *Clin Positron Imaging.* 1999;2:159–171.
28. Pak K, Cheon GJ, Nam HY, et al. Prognostic value of metabolic tumor volume and total lesion glycolysis in head and neck cancer: a systematic review and meta-analysis. *J Nucl Med.* 2014;55:884–890.
29. Lee JW, Kang CM, Choi HJ, et al. Prognostic value of metabolic tumor volume and total lesion glycolysis on preoperative ^{18}F-FDG PET/CT in patients with pancreatic cancer. *J Nucl Med.* 2014;55:898–904.
30. Ulaner GA, Eaton A, Morris PG, et al. Prognostic value of quantitative fluorodeoxyglucose measurements in newly diagnosed metastatic breast cancer. *Cancer Med.* 2013;2:725–733.
31. Burger IA, Casanova R, Steiger S, et al. FDG-PET/CT of non-small cell lung carcinoma under neo-adjuvant chemotherapy: background based adaptive volume metrics outperform TLG and MTV in predicting histopathological response. *J Nucl Med.* 2016;57:849–854.
32. Bütof R, Hofheinz F, Zöphel K, et al. Prognostic value of SUR in patients with trimodality treatment of locally advanced esophageal carcinoma. *J Nucl Med.* 2018;60:192–198.
33. Shin S, Pak K, Kim IJ, et al. Prognostic value of tumor-to-blood standardized uptake ratio in patients with resectable non-small-cell lung cancer. *Nucl Med Mol Imaging.* 2017;51:233–239.
34. Hofheinz F, Bütof R, Apostolova I, et al. An investigation of the relation between tumor-to-liver ratio (TLR) and tumor-to-blood standard uptake ratio (SUR) in oncological FDG PET. *EJNMMI Res.* 2016;6:19.
35. Barrington SF, Qian W, Somer EJ, et al. Concordance between four European centres of PET reporting criteria designed for use in multicentre trials in Hodgkin lymphoma. *Eur J Nucl Med Mol Imaging.* 2010;37:1824–1833.
36. Hasenclever D, Kurch L, Mauz-Körholz C, et al. qPET: a quantitative extension of the Deauville scale to assess response in interim FDG-PET scans in lymphoma. *Eur J Nucl Med Mol Imaging.* 2014;41:1301–1308.
37. Wahl RL, Jacene H, Kasamon Y, et al. From RECIST to PERCIST: evolving considerations for PET response criteria in solid tumors. *J Nucl Med.* 2009; 50(suppl 1):122S–150S.
38. O JH, Lodge MA, Wahl RL. Practical PERCIST: a simplified guide to PET response criteria in solid tumors 1.0. *Radiology.* 2016;280:576–584.
39. Barrington SF, Kluge R. FDG PET for therapy monitoring in Hodgkin and non-Hodgkin lymphomas. *Eur J Nucl Med Mol Imaging.* 2017;44:97–110.
40. Sprinz C, Zanon M, Altmayer S, et al. Effects of blood glucose level on ^{18}F fluorodeoxyglucose (^{18}F-FDG) uptake for PET/CT in normal organs: an analysis on 5623 patients. *Sci Rep.* 2018;8:2126.
41. Lindholm H, Brolin F, Jonsson C, et al. The relation between the blood glucose level and the FDG uptake of tissues at normal PET examinations. *EJNMMI Res.* 2013;3:50.
42. Kubota K, Watanabe H, Murata Y, et al. Effects of blood glucose level on FDG uptake by liver: a FDG-PET/CT study. *Nucl Med Biol.* 2011;38:347–351.
43. Malladi A, Viner M, Jackson T, et al. PET/CT mediastinal and liver FDG uptake: effects of biological and procedural factors. *J Med Imaging Radiat Oncol.* 2013;57:169–175.
44. Groheux D, Delord M, Rubello D, et al. Variation of liver SUV on ^{18}F-FDG PET/CT studies in women with breast cancer. *Clin Nucl Med.* 2013;38:422–425.
45. Webb RL, Landau E, Klein D, et al. Effects of varying serum glucose levels on ^{18}F-FDG biodistribution. *Nucl Med Commun.* 2015;36:717–721.
46. Eskian M, Alavi A, Khorasanizadeh M, et al. Effect of blood glucose level on standardized uptake value (SUV) in ^{18}F-FDG PET-scan: a systematic review and meta-analysis of 20,807 individual SUV measurements. *Eur J Nucl Med Mol Imaging.* 2019;46:224–237.
47. Alkhawaldeh K, Bural G, Kumar R, et al. Impact of dual-time-point ^{18}F-FDG PET imaging and partial volume correction in the assessment of solitary pulmonary nodules. *Eur J Nucl Med Mol Imaging.* 2008;35:246–252.
48. Laffon E, de Clermont H, Begueret HV, et al. Assessment of dual-time-point ^{18}F-FDG-PET imaging for pulmonary lesions. *Nucl Med Commun.* 2009;30:455–461.
49. Tian R, Su M, Tian Y, et al. Dual-time point PET/CT with F-18 FDG for the differentiation of malignant and benign bone lesions. *Skeletal Radiol.* 2009;38:451–458.
50. Imbriaco M, Caprio MG, Limite G, et al. Dual-time-point ^{18}F-FDG PET/CT versus dynamic breast MRI of suspicious breast lesions. *AJR.* 2008;191:1323–1330.
51. Kim DW, Jung SA, Kim CG, et al. The efficacy of dual time point F-18 FDG PET imaging for grading of brain tumors. *Clin Nucl Med.* 2010;35:400–403.
52. Mavi A, Urhan M, Yu JQ, et al. Dual time point ^{18}F-FDG PET imaging detects breast cancer with high sensitivity and correlates well with histologic subtypes. *J Nucl Med.* 2006;47:1440–1446.
53. Herholz K, Rudolf J, Heiss WD. FDG transport and phosphorylation in human gliomas measured with dynamic PET. *J Neurooncol.* 1992;12:159–165.
54. Dimitrakopoulou-Strauss A, Pan L, Strauss LG. Quantitative approaches of dynamic FDG-PET and PET/CT studies (dPET/CT) for the evaluation of oncological patients. *Cancer Imaging.* 2012;12:283–289.
55. Sokoloff L, Smith CB. Basic principles underlying radioisotopic methods for assay of biochemical processes in vivo. In: Greitz T, Ingvar DH, Widen L, eds. The metabolism of the human brain studied with positron emission tomography. New York, NY: Raven Press; 1983:123–148.
56. Patlak CS, Blasberg RG. Graphical evaluation of blood-to-brain transfer constants from multiple-time uptake data: generalizations. *J Cereb Blood Flow Metab.* 1985;5:584–590.
57. Kajáry K, Lengyel Z, Tőkés AM, et al. Dynamic FDG-PET/CT in the initial staging of primary breast cancer: clinicopathological correlations. *Pathol Oncol Res.* April 3, 2019 [Epub ahead of print].
58. Ye Q, Wu J, Lu Y, et al. Improved discrimination between benign and malignant LDCT screening-detected lung nodules with dynamic over static ^{18}F-FDG PET as a function of injected dose. *Phys Med Biol.* 2018;63:175015.
59. Okazumi S, Dimitrakopoulou-Strauss A, Schwarzbach MH, et al. Quantitative, dynamic ^{18}F-FDG-PET for the evaluation of soft tissue sarcomas: relation to differential diagnosis, tumor grading and prediction of prognosis. *Hell J Nucl Med.* 2009;12:223–228.